Gyrokinetic Simulation of Kinetic Ballooning Mode and Its Parametric Stabilization in Tokamak Plasmas With Impurities

Yong Shen, Jia-Qi Dong, and Jia Li

***Abstract*— Kinetic ballooning mode (KBM) and its parametric stabilization in tokamaks are studied qualitatively by means of gyrokinetic simulation. The circular magnetic tokamak discharge with the Shafranov shift is considered and the $\hat{s} - \alpha$ model equilibrium is employed. The kinetic characteristics of ions, such as Landau resonance, magnetic drift, and finite Larmor radius (FLR) are all taken into account. The full ion transit and toroidal drift effects are retained. Impurity effect is also included. As a result, the existence of, and approaching way to the second KBM stable regime were identified. It was first revealed that impurities play a role of stabilizing when the impurity density profile peaks in the same direction as those of the electron and main ion density profiles, owing to that compressibility effects is weakened. It shows that the mode maximum growth rate appears at the turning point of magnetic shear $\hat{s}_c = q/4 - q/2$, while the formula can be modified due to other plasma parameters such as η_i and impurity species. Some parametric stabilizations of KBM are suggested, including the accumulation of impurities toward the plasma center; and entering or approaching to the second stable regime by means of making the electron density or ion/electron temperature gradients high enough, by which the internal or edge transport barrier (ITB/ETB) is anticipated to be formed in many cases. In addition, we showed that the artificial control of safety factor and magnetic shear was also beneficial to the stabilization of ballooning mode.**

***Index Terms*— Gyrokinetic simulation, impurity effect, kinetic ballooning mode (KBM), magnetic shear, parametric stabilization, second stable regime.**

I. Introduction

THE performance of the fusion plasma confinement is largely determined by various kinks of instabilities. The ballooning mode is widely believed to be one of the fundamental instabilities in a tokamak [1], [2]. A short wavelength ballooning mode can determine the maximum pressure and generate cross-field thermal and particle transport at the plasma core and edge regions [3], [4], and many current hot topics of fusion research involve ballooning instability. First, the ballooning mode plays a significant role in driving turbulence near the plasma edge [5], [6], [7], and plays a key role in edge transport. Saarelma et al. [8] found that ballooning instability prevented the H-mode access in plasmas with negative triangularity shape on the DIII-D tokamak. And Eich et al. [9] showed the H-mode density limit might be set by ballooning stability at the separatrix for JET and ASDEX Upgrade. Second, in addition to the ordinary ballooning modes [10], [11], [12], [13], [14], [15], [16], some new ballooning modes have now been explored, which have special significance in fusion experiments. For instance, in order to mitigate the possible harmful heat load from edge localized modes (ELMs) in the high confinement mode (H mode) in future fusion devices, it is necessary to suppress or to mitigate the ELMs. A type-I ELM can be regarded as a short wavelength ballooning mode or peeling-ballooning mode [17]. Besides, field-line localized ballooning modes have been observed at the edge of high confinement mode plasmas in ASDEX Upgrade [18]. Third, there are inherent relations between ballooning mode and other microscopic instabilities. For example, the type of edge turbulence transition from resistive ballooning modes (RBMs) to drift-type ion temperature gradient (ITG) modes has been observed on the HL-2A tokamak [19]. Dubuit et al. [20] showed the magnetic island generation by remote ballooning turbulence close to the plasma edge. Therefore, in the research of some key issues, further analysis of the characteristics and stabilization of ballooning mode needs to be carried out simultaneously.

Characterizing the nature of ballooning instability is of significant importance for understanding the underlying physics of turbulent transport in tokamak plasmas, both in magneto-hydrodynamic (MHD) and kinetic theory. Kinetic ballooning modes (KBMs) are excited by the curvature of the confining magnetic field and the plasma pressure gradient. The stabilization and destabilization factors in kinetic effects have been partially involved in previous works [21], [22], [23], [24]. It is commonly believed [22], [23] that finite Larmor radius (FLR) effect is stabilizing while ion magnetic drift resonance is destabilizing. When temperature gradients are considered, the stability boundary may change fundamentally due to the introduction of a new source of free energy independent of the MHD drive. Results of linear numerical simulations [24] showed that finite compressibility destabilized ballooning modes which were otherwise stable due to the ion diamagnetic drift effect. The numerical method is used to simulate quantitatively and measure the characteristics of

Manuscript received 14 March 2023; revised 17 May 2023 and 24 June 2023; accepted 2 August 2023. Date of publication 22 August 2023; date of current version 1 September 2023. This work was supported in part by the National Natural Science Foundation of China under Grant 12075077 and in part by the National Key Research and Development Program of China under Grant 2017YFE0301200 and Grant 2019YFE03050003. The review of this article was arranged by Senior Editor S. J. Gitomer. *(Corresponding author: Yong Shen.)*

Yong Shen and Jia-Qi Dong are with the Southwestern Institute of Physics, Chengdu 610041, China (e-mail: sheny@swip.ac.cn; jiaqi@swip.ac.cn).

Jia Li is with the School of Mathematics and Science, Chengdu University of Technology, Chengdu 610059, China (e-mail: lijia@swip.ac.cn).

Color versions of one or more figures in this article are available at https://doi.org/10.1109/TPS.2023.3303420.

Digital Object Identifier 10.1109/TPS.2023.3303420

the ballooning mode under kinetic effects. The calculated results, such as the mode growth rate and real frequency as well as wavenumber spectrum, are of great significance to the quantification of the scale of the transport driven by ballooning mode induced turbulence, the latter of which still remains the most challenging problems for the present plasma theory and experiments.

The extended instability [25], which refers to the KBM instability in the second stable regime of ideal MHD ballooning mode, is shown to be a plausible candidate for the low-k broadband fluctuation recently observed in the wide-pedestal quiescent-H (QH) mode of DIII-D [26]. The study [25] shows that this extended instability is caused by two parametric effects, say, the effects of ITG (η_i) and impurity. In fact, the multiple parametric effects on KBM in tokamaks are an enduring topic, which is often closely related to the destabilization and stabilization of ballooning mode instability. In the study of parametric stabilization, in addition to η_i effect [27], the impurity problem was recognized mostly important due to its inevitability in tokamaks and its influence on plasma confinement [28], [29], [30]. Impurity effect on micro-instability is an important subject in fusion research. Impurity impacts on drift wave stability and impurity transport have been studied (e.g., see [31], [32], [33]) in recent decades. It is also necessary to further survey impurity impacts on KBM, which encouraged us to take it as one of the research contents of this article. Impurity effect is probably correlated to the "peaking direction" of impurity density. Here, assuming that the impurity density has a peaking distribution in the plasma, when the impurity density profile peaks in the same direction as those of the electron and main ion density profiles, we say that the peaking direction of impurity density profile is positive. Conversely, when the impurity density profile peaks opposite to those of the electron and main ion density profiles, its peaking direction is negative. In this article, we only study the former.

In addition to the impurity effect, the electron density gradient may also be closely related to KBM instability, and the roles of safety factor and magnetic shear are also deserved attention in studies. In this article, we will study these topics deliberately by means of gyrokinetic simulation. The research involves analysis of the main parameter effects and parametric stabilization of KBM. This work covers almost all major kinetic effects except compression effects. This is the method adopted by most previous studies [10], [11], [12], [13], [14], [15], [16], so it is deserved to give ones a comprehensive numerical result to link the previous research and the new study including complete electromagnetic effect together, the latter of which will be done in our next work. However, although the compression effect has no qualitative impact on the properties of ballooning modes, it has a small impact on it quantitatively. Therefore, the work of this article is oriented to "qualitatively study" on KBMs. We focus on the analysis related to the mode maximum growth rate, which can minimize the quantitative effect of parallel magnetic perturbation on the mode growth rate. The results show the existence of the second stable region of KBM and the way to approach it, and the stabilizing effect of impurities was observed for the first time. Some parametric stabilizations of KBM are observed.

The remainder of this article is organized as follows. The physics models and mathematical solver are presented in Section II. Numerical schemes and results are described in Section III, where the KBMs are analyzed deliberately and its parametric stabilization is studied, and Section IV is devoted to conclusions.

II. Physical Model and Mathematical Solver

We consider the circular magnetic tokamak discharge of the circular magnetic flux surface with the Shafranov shift and the $\hat{s}-\alpha$ model [34] equilibrium is employed. Here, the pressure parameter $\alpha = -Rq^2 d\beta/dr$, with β being the ratio of thermal to magnetic pressures, and R and r the major and minor radii of plasma, respectively. The perturbed electric field is presented by both the scalar potential $\tilde{\phi}$ and parallel vector potential $\tilde{A}_{||}$. The kinetic characteristics of ions, such as Lamdau resonance, magnetic drift, and FLR are all taken into account. The full ion transit and toroidal drift effects are retained. Impurity effect is included. In this article, H^+ ions are considered as the main ion species. The electrons are considered massless, highly toroidally transiting without collision and trapping effects. The effect of parallel magnetic fluctuations $\delta B_{||}$ was ignored in the calculations, which, in fact, does not qualitatively affect the correctness of the results regarding KBM in tokamaks with $\hat{s}-\alpha$ model.

Coupled equations governing behaviors of the eigenmodes in the system can be given [35] from charge neutrality

$$\tilde{n}_e = \tilde{n}_i + Z_z \tilde{n}_z \tag{1}$$

with

$$\tilde{n}_s = \int g_s d^3\boldsymbol{v} \tag{2}$$

and the parallel component of Ampere's law

$$\nabla_\perp^2 \tilde{A}_{||} = -\frac{4\pi}{c}\left(\tilde{j}_{e||} + \tilde{j}_{i||} + \tilde{j}_{c||}\right) \tag{3}$$

with

$$\tilde{j}_{s||} = q_s \int v_{||} g_s d^3\mathbf{v}. \tag{4}$$

Here, Z_s is the charge number of the species $s = i, z$, and e, for hydrogen ions, impurity ions, and electrons, respectively. $\tilde{n}_s$ is the perturbed density

$$g_s = -\frac{q_s F_{Ms}}{T_s}\tilde{\phi} + h_s J_0(\delta_s) \tag{5}$$

is the nonadiabatic response of the distribution function and T_s is charge and temperature of the particle species s. J_0 is the Bessel function of zeroth order. $\delta_s = \hat{v}_\perp (2b_s)^{1/2}$, $2b_s = k_\perp^2 v_{ts}^2/\Omega_s^2$, and $\Omega_s = Z_s B/m_s c$ is the gyrofrequency of ion species s. The Maxwellian equilibrium distribution $F_{Ms} = n_{0s}(\pi v_{ts}^2)^{-3/2}\exp(-v^2/v_{ts}^2)$ is employed. The nonadiabatic response h_s is determined by solving the 1-D gyrokinetic equation in the ballooning representation

$$i\frac{v_\parallel}{qR_0}\frac{\partial}{\partial\theta}h_s + (\omega-\omega_{Ds})h_s = (\omega-\omega_{*sT})J_0(\delta_s)F_{Ms}\times\frac{Z_s}{T_s}\left(\hat{\phi}(\theta) - \frac{v_\parallel}{c}\hat{A}_\parallel(\theta)\right) \tag{6}$$

where θ is the extended poloidal angle, and $\omega_{Ds} = 2\varepsilon_n\omega_{*sT}$ $[\cos\theta + \sin\theta(\hat{s}\theta - \alpha\sin\theta)]\times(v_{||}^2/v_{ts}^2 + v_\perp^2/2v_{ts}^2)$, $\omega_{*sT} = \omega_{*s}$

$[1+\eta_s(v^2/v_{ts}^2-3/2)]$ with $\varepsilon_n = L_{ne}/R$, $\eta_s = L_{ns}/L_{Ts}$, $\omega_{*s} = ck_\theta T_s/Z_s B L_{ns}$ is the diamagnetic drift frequency, k_θ the poloidal wave vector of the perturbations, and the density and temperature inhomogeneity are introduced in terms of the gradient scale length, and $L_{ns} = -(d\ln n_s/dr)^{-1}$, $L_{Ts} = -(d\ln T_s/dr)^{-1}$. Equation (6) can be solved with the asymptotic decaying boundary condition $h_s(\theta) = 0$ as $\theta \to -\mathrm{sgn}(v_{||})\infty$.

We can derive the following coupled integral equations from (1) and (3) after straightforward algebra:

$$\begin{aligned}&\left[1+\tau_i Z_i f_i+\tau_z Z_z f_z\right]\hat{\Phi}(k)\\&=\int_{-\infty}^{+\infty}\frac{dk'}{\sqrt{2\pi}}\Big\{\left[K_{11}^i(k,k')+K_{11}^z(k,k')\right]\hat{\Phi}(k')\\&\quad+\left[K_{12}^i(k,k')+K_{12}^z(k,k')+K_{12}^e(k,k')\right]\\&\quad\times\hat{A}_{||}(k')\Big\}\end{aligned}\tag{7}$$

$$\begin{aligned}&\frac{k_\perp^2}{2}\hat{A}_{||}(k')\\&=\int_{-\infty}^{+\infty}\frac{dk'}{\sqrt{2\pi}}\Big\{\left[K_{21}^i(k,k')+K_{21}^z(k,k')+K_{21}^e(k,k')\right]\hat{\Phi}(k')\\&\quad+\left[K_{22}^i(k,k')+K_{22}^z(k,k')+K_{22}^e(k,k')\right]\\&\quad\times\hat{A}_{||}(k')\Big\}\end{aligned}\tag{8}$$

where $\hat{\Phi}(k)$ and $\hat{A}_{||}(k)$ are the Fourier components of $\tilde{\phi}$ and $(v_{ti}/c)\tilde{A}_{||}(r)$, respectively, for the mode structures in the ballooning space; $\tau_s = T_e/T_s$, $f_i = 1-f_z$, with $f_z = Z_z n_z/n_e$, $Z_i = 1$, $Z_z = Z$. The mode frequency $\omega(=\omega_r+i\gamma)$ is normalized to electron diamagnetic drift frequency ω_{*e}, the wavenumbers k, k'

$$K_{12}^e(k,k') = \frac{iq\sqrt{\pi\tau_i}}{2\sqrt{2}\varepsilon_n\hat{s}}(\hat{\omega}-1)\mathrm{sgn}(k-k')\tag{9}$$

$$K_{21}^e(k,k') = -\frac{\beta_e}{\tau_i}K_{12}^e(k,k')\tag{10}$$

$$\begin{aligned}K_{22}^e(k,k') = \beta_e\Bigg\{&\frac{-\sqrt{\pi}}{4\sqrt{2}}\left(\frac{q}{\varepsilon_n\hat{s}}\right)^2\hat{\omega}(\hat{\omega}-1)|k-k'|+\frac{\sqrt{\pi}q^2k_\theta}{2\sqrt{2}\varepsilon_n\hat{s}}\\&\times\left[\hat{\omega}-(1+\eta_e)\right]\mathrm{sgn}(k-k')g(\theta,\theta')\Bigg\}.\end{aligned}\tag{11}$$

And

$$K_{mn}^u(k,k') = -i\int_{-\infty}^{0}\omega_{*e}d\tau H_{mn}^u(\tau,k,k')\tag{12}$$

for $u = i, z$, $m = 1, 2$ and $n = 1, 2$. Here (see Appendix)

$$\begin{aligned}&H_{11}^u(\tau,k,k')\\&=\frac{\sqrt{2}\ f_u e^{-i\omega\tau}}{\sqrt{a_u}(1+a_u)\sqrt{\lambda_u}}\exp\left[-(k-k')^2/4\lambda_u\right]\\&\quad\times\Bigg\{\frac{\omega}{\omega_{*e}}Z_u\tau_u+L_{eu}\Bigg[1-\frac{3\eta_u}{2}+\frac{2\eta_u}{1+a_u}\\&\qquad\times\left[1-\frac{(k_\perp^2+k_\perp'^2)\mu_u}{2(1+a_u)\tau_u Z_u^2}+\frac{k_\perp k_\perp'\mu_u}{(1+a_u)\tau_u Z_u^2}\frac{I_{1u}}{I_{0u}}\right]\\&\qquad+\frac{\eta_u(k-k')^2}{4a_u\lambda_u}\Bigg]\Bigg\}\Gamma_{0u}(k_\perp,k_\perp')\end{aligned}\tag{13}$$

$$\begin{aligned}&H_{12}^u(\tau,k,k')\\&=\frac{1}{2\sqrt{a_u\lambda_u}}\cdot\frac{\sqrt{\tau_i}}{\sqrt{\tau_u\mu_u}}(k-k')H_{11}^u(\tau,k,k')\end{aligned}\tag{14}$$

$$\begin{aligned}&H_{21}^u(\tau,k,k')\\&=-\frac{\beta_e}{2\sqrt{a_u\lambda_u}}\cdot\frac{1}{\sqrt{\tau_i\tau_u\mu_u}}(k-k')H_{11}^u(\tau,k,k')\end{aligned}\tag{15}$$

$$\begin{aligned}&H_{22}^u(\tau,k,k')\\&=-\frac{\beta_e}{4a_u\lambda_u}\cdot\frac{1}{\tau_u\mu_u}(k-k')^2H_{11}^u(\tau,k,k')\end{aligned}\tag{16}$$

where

$$\lambda_u = \frac{\tau^2\omega_{*e}^2}{\tau_u a_u\mu_u}\left(\frac{\hat{s}}{q}\varepsilon_n\right)^2,\quad a_u = 1+\frac{i2\varepsilon_n\omega_{*e}\tau}{\tau_u Z_u}\times\frac{g(\theta,\theta')}{\theta-\theta'}$$

$$I_{ou} = I_0\left(\frac{k_\perp k_\perp'\mu_u}{(1+a_u)\tau_u Z_u^2}\right)$$

$$\Gamma_{0u} = I_0\left(\frac{k_\perp k_\perp'\mu_u}{(1+a_u)\tau_u Z_u^2}\right)\exp\left[-\frac{(k_\perp^2+k_\perp'^2)\mu_u}{2(1+a_u)\tau_u Z_u^2}\right]$$

$$k = k_\theta\hat{s}\theta,\quad k' = k_\theta\hat{s}\theta',\quad k_\perp^2 = k_\theta^2+k^2$$

$$k_\perp'^2 = k_\theta^2+k'^2,\quad \varepsilon_n = \frac{L_{ne}}{R},\quad \eta_u = \frac{L_{nu}}{L_{Tu}}$$

$$L_{eu} = \frac{L_{ne}}{L_{nu}},\quad \mu_u = m_u/m_i$$

and $g(\theta,\theta') = (\hat{s}+1)(\sin\theta-\sin\theta')-\hat{s}(\theta\cos\theta-\theta'\cos\theta')-(\alpha/2)(\theta-\theta'-\sin\theta\cos\theta+\sin\theta'\cos\theta')$.

Here, note that the values of L_{ei} and η_z are not the primary parameters in the calculations because due to the quasi-neutrality condition, L_{ei} is not independent, in fact

$$L_{ei} = \frac{1-f_z L_{ez}}{1-f_z}.$$

Besides, in the assumption $T_i(r) = T_z(r)$, we have

$$\eta_z = \frac{\eta_i\left[(L_{nz}/L_{ne})-f_z\right]}{1-f_z}.$$

Equations (7) and (8) constitute the set of eigenvalue equations for ITG and KBMs. If $\beta_e \to 0$, the ITG mode remains unstable only. Increasing β_e makes ITG mode stabilized, only KBM may be unstable. We have solved the set of equations using the Rayleigh-Ritz method by upgraded numerical code HD7 [35], [36], [37]. The numerical results deliberately show the comprehensive properties of KBMs in tokamak plasmas.

III. Numerical Results

The KBMs are first simulated when the temperature gradient is ignored in the plasma in the absence of impurity ions as the baseline for comparison. In a pure hydrogen plasma (i.e., $f_z = 0$) with $\eta_i = 0$, the dependences of the normalized growth rate and real frequency of the mode on β_e (electron β) and α are shown in Fig. 1, where four cases are illustrated, including the case with $q = 1.2$, $\hat{s} = 0.2$; the case with $q = 2$, $\hat{s} = 1$, and the cases with $q = 4$, $\hat{s} = 1$, and $\hat{s} = 2$. Here, $\eta(\equiv\eta_i = \eta_e) = 0$ is assumed. The other parameters are $\varepsilon_n = 0.2, k_\theta\rho_s = 0.3$, $\tau_i = 1$. The results show that the mode characteristics are very similar to that of ideal MHD ballooning mode [1] because for $\eta_i = 0$, the eigenmode equations for KBM reduce to the ideal MHD

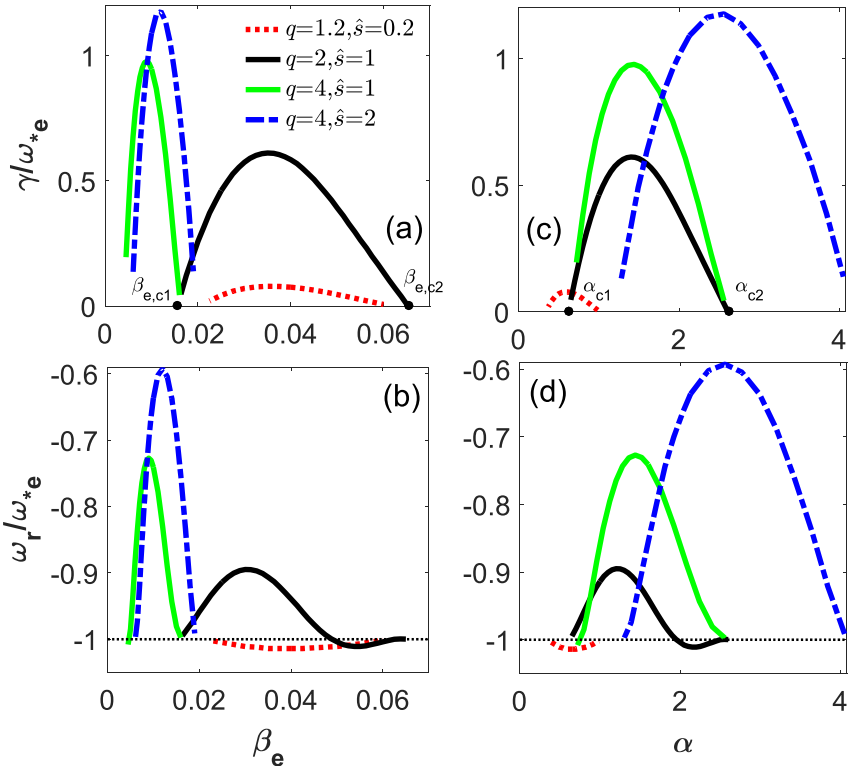

Fig. 1. Dependence of the (a) and (c) normalized growth rate γ/ω_{*e} and (b) and (d) real frequency ω_r/ω_{*e} of ballooning modes on (a) and (b) β_e or (c) and (d) α. Here, $f_z = 0$ and $\eta_i = \eta_e = 0$. The other parameters are $\varepsilon_n = 0.2$, $k_\theta \rho_s = 0.3$, $\tau_i = 1$.

ballooning equation in marginal stability regime at $\omega_r = \omega_{*i}$, and therefore, we call these modes as "MHD-like" ballooning modes. The critical β for the instabilities appears at $\omega_r = \omega_{*i}$, which is the same as that for ideal MHD ballooning modes and independent of FLR and magnetic drift resonance effects.

With the comparisons among the four cases in Fig. 1, we can see an important property of the MHD-like ballooning mode. That is, for the higher safety factor q, the mode maximum growth rate is higher and the threshold values α_{c1} and α_{c2} (for the first and second ideal MHD stable regimes, respectively) are also higher, while the threshold values $\beta_{e,c1}$ and $\beta_{e,c2}$ are lower. It is demonstrated that with the increase of magnetic shear $\hat{s}$, the critical α for the ideal MHD stable regimes increase. Moreover, when the q value is changed from 2 (the black solid line) to 4 (the green solid line), or when the $\hat{s}$ value is changed from 1 (the green solid line) to 2 (the blue dashed-dotted line) and the other parameters remain unchanged, there is no occurrence of extended instability [25] in both β_e and α spaces, but only from one MHD-like ballooning mode to another similar one. That is, from Fig. 1, we can conclude that merely increasing q or $\hat{s}$ may not change the attributes of the MHD-like ballooning mode. Furthermore, it is suggested that the safety factor and magnetic shear are not the drives for the generation of the extended instability in the second ideal MHD stable regime. However, as $\eta_i = 1$, the extended instability occurs, as shown in Fig. 2.

Plotted in Fig. 2 are the normalized growth rates (a) and (c) and real frequencies (b) and (d) of the modes as functions of β_e (a) and (b) and α (c) and (d) for $q = 2, 4$ and $\eta = 0, 1$ to study the effects of η_i on the mode in a pure hydrogen plasma. We see that the first critical β_e and α for the ideal MHD stable regime for the case with $q = 2$ and $\eta = 0$ (the black solid line) are $\beta_{e,c1} \cong 0.012$ and $\alpha_{c1} \cong 0.45$, respectively, as also seen in Fig. 1. While the left critical β_e and α where the growth rate vanishes for the case of $q = 2$ and $\eta = 1$ (the black dashed line) are significantly less than the thresholds for the first ideal MHD stable regime, $\beta_{e,c1}$ and α_{c1}, respectively. More evidently, however, the second critical β_e and α become much higher than the thresholds for the second ideal MHD stable regimes, $\beta_{e,c2}$ and α_{c2}, respectively. These mean that the extended instability occurs in the second ideal MHD stable regime for the cases $\eta_i = 1$. In addition, as $\eta_i = \eta_e = 0$, the normalized real frequency ω_r/ω_{*e} weakly depends on β_e and α, whilst for $\eta_i = \eta_e = 1$, the real frequency strongly depends on both β_e and α, as shown in Fig. 2(b) and (d). In a word, the occurrence of extended instability mainly depends on ion inverse Lamdau damping (when $\eta_i \gtrsim 1$ is active) or other causes (e.g., impurity effect (also see [25]).

In the following work, some parametric effects on KBM are surveyed as η_i and η_e are nonzero. In order to demonstrate evidently the physical properties of the mode, we study the KBMs at a specific β_e where the peak growth rate is obtained. The values of some key parameters, such as q, $\hat{s}$, η_i, η_e, f_z, and β_e, are listed in Table I. Other parameters are assumed as $\varepsilon_n = 0.2, k_\theta \rho_s = 0.3$, $\tau_i = 1$, unless otherwise stated. And for the impurity case, $L_{ez} = 1 > 0$, $f_z = 0.3$, $\tau_z = 1$, and C^{6+} impurity ion is considered. Here, note that the peaking direction of impurity density profile is inward, corresponding to $L_{ez} > 0$. On the contrary, if the impurity density profile is

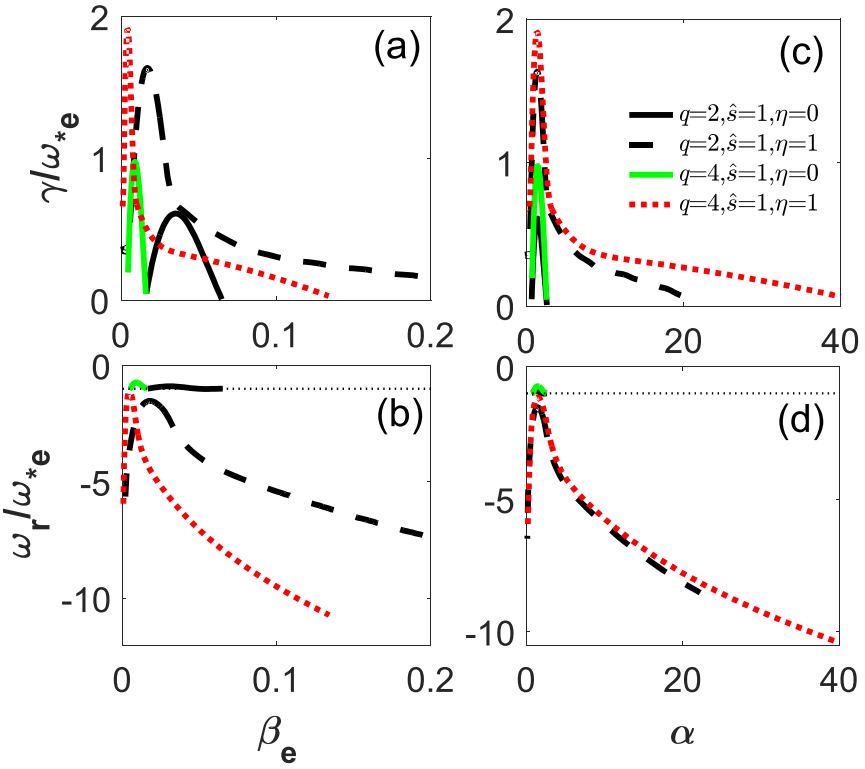

Fig. 2. In pure hydrogen plasmas, (a) and (c) normalized growth rates and (b) and (d) real frequencies of the modes as functions of (a) and (b) β_e or (c) and (d) α for deferent q and η. The other parameters are the same as that in Fig. 1.

TABLE I

PARAMETERS FOR FIVE TYPICAL CASES. HERE $\eta \equiv \eta_i = \eta_e$, AND OTHER PARAMETERS ARE $\varepsilon_n = 0.2$, $k_\theta \rho_s = 0.3$, $\tau_i = 1$; FOR THE CASE $f_z = 0.3$, C^{6+} IMPURITY ION IS CONSIDERED

Case series	q	$\hat{s}$	η	f_z	β_e
Case 1	2	1	1	0	0.0175
Case 2	4	1	1	0	0.004
Case 3	4	2	1	0	0.0075
Case 4	4	2	2	0	0.005
Case 5 (C^{6+})	2	1	1	0.3	0.0175

peaked outward and opposite to that of the electron and main ion density profiles, we have $L_{ez} < 0$.

The impurity effect is illustrated in Fig. 3 for different η, q, and $\hat{s}$ parameters. Here, we plot the normalized growth rate γ/ω_{*e} and real frequency ω_r/ω_{*e} as functions of f_z. It can be seen in the figure that the dependence of real frequency on f_z is monotonically decreasing for f_z increasing when $L_{ez} = 1 > 0$,. When $\eta_i = \eta_e = 1$ or 2, the instability growth rate decreases with the increase of impurity charge concentration f_z, implying that the role of impurity ions is stabilizing. The larger the q or $\hat{s}$ or η, the faster the mode growth rate decreases. It means that the larger q or $\hat{s}$ or η_i (and η_e), the stronger the stabilizing effect of the impurities on the mode is, although the figure also shows that the instability growth rate may be actually higher for larger q or s or η_i at a certain fixed f_z. This is because the presence of impurities weakens the finite compression effect [23], thus contributing to the stabilization of the KBM, and the increase of q or η_i enhance this impurity effect.

The electron density gradient is one of the key factors that determine the plasma pressure gradient. The dependence of mode eigenvalue on the electron density gradient parameter is shown in Fig. 4. It should be noted that here $\varepsilon_n = L_n/R$, say, the value ε_n is inversely proportional to the electron density gradient. Fig. 4(a) shows the dependence of the mode growth rate on the electron density gradient parameter $(1/\varepsilon_n)$, and Fig. 4(c) shows the variation of the mode growth rate in the pressure gradient (α) space, where the α value changes with electron density gradient. Fig. 4(b) and (d) shows the normalized real frequency against $1/\varepsilon_n$ and α, respectively. Obviously, the strength and variation of KBM instability are significantly dependent on electron density gradient. At first, the normalized growth rate γ/ω_{*e} increases rapidly from the lower density gradient threshold $[1/\varepsilon_n]_{c1} \sim 1.5 - 2.5$, and then reaches the peak growth rate at the critical gradient $[1/\varepsilon_n]_c \sim 5$, then followed by a rapid declines rapidly with the further increase of $1/\varepsilon_n$, and finally vanishes at the higher density threshold $[1/\varepsilon_n]_{c2}$. The safety factor q and η_i have impacts on these threshold values. The bigger

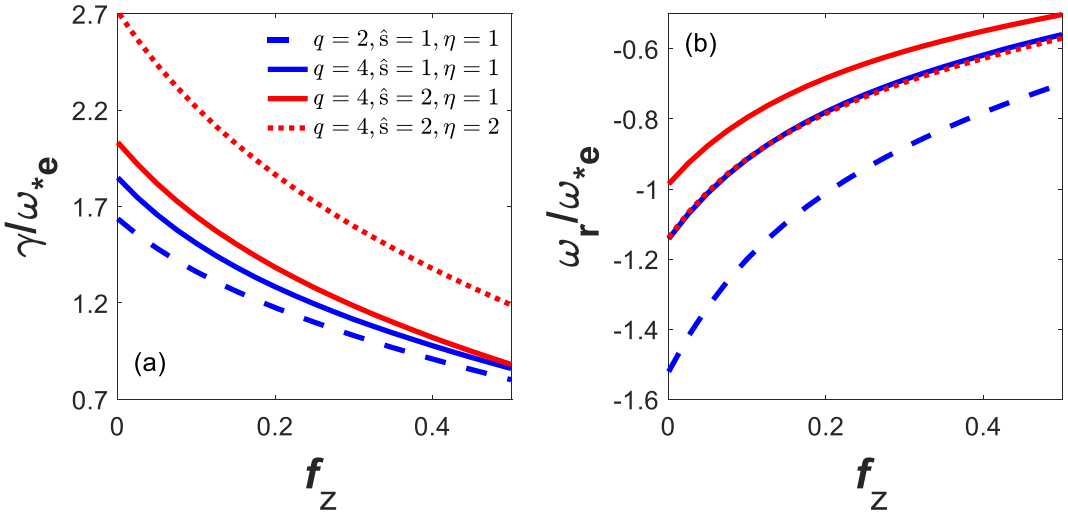

Fig. 3. Impurity effect. Dependence of (a) normalized growth rate and (b) real frequency on f_z for deferent values of q, $\hat{s}$ and $\eta(\equiv\eta_i = \eta_e)$. For other parameters of each case, please refer to Table I.

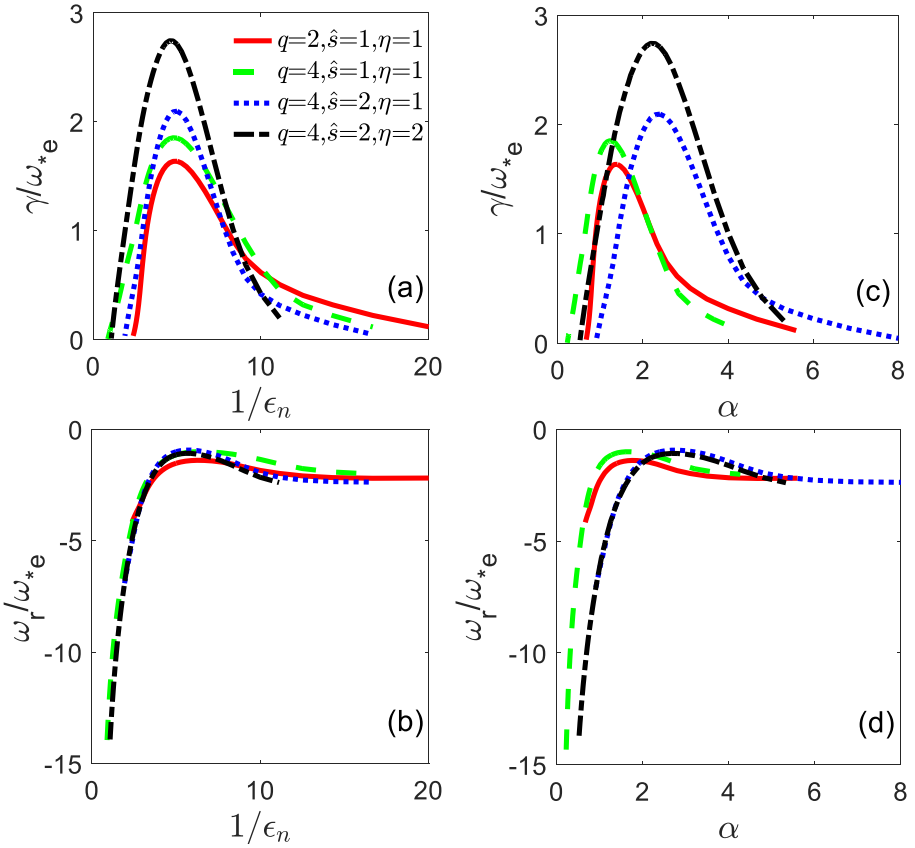

Fig. 4. Dependence of the mode eigenvalue on (a) and (b) $1/\varepsilon_n$ and (c) and (d) α for different case of q, $\hat{s}$, and η. The other parameters are defined in Table I for each case.

q or η_i is, the smaller $[1/\varepsilon_n]_{c1}$ and $[1/\varepsilon_n]_{c2}$ are. There are $[1/\varepsilon_n]_{c2} \sim 12, 16, 17,$ and 22 (as estimated), respectively, for the four cases shown in the figure. In the regimes of smaller ($[1/\varepsilon_n]_{c1} \leq 1/\varepsilon_n \leq [1/\varepsilon_n]_c$) and larger ($[1/\varepsilon_n]_c < (1/\varepsilon_n) \leq [1/\varepsilon_n]_{c2}$) electron density gradient regions, the density gradient plays the roles of destabilizing and stabilizing, respectively, while in the regime region of very small electron density gradient ($(1/\varepsilon_n) < [1/\varepsilon_n]_{c1}$) or very large electron density region ($(1/\varepsilon_n) > [1/\varepsilon_n]_{c2}$), the KBM is completely stabilized. This is consistent with the judgment that the mode has the first and second KBM stable regimes. If the case that only electron density gradient causes the occurrence of the KBM stable regimes is assumed, and the effect of temperature gradient is ignored, then in the first stable region ($(1/\varepsilon_n) < [1/\varepsilon_n]_{c1}$), the mode real frequency is very high, and $|\omega_r/\omega_{*e}| \sim O(10)$. In the second KBM stable region

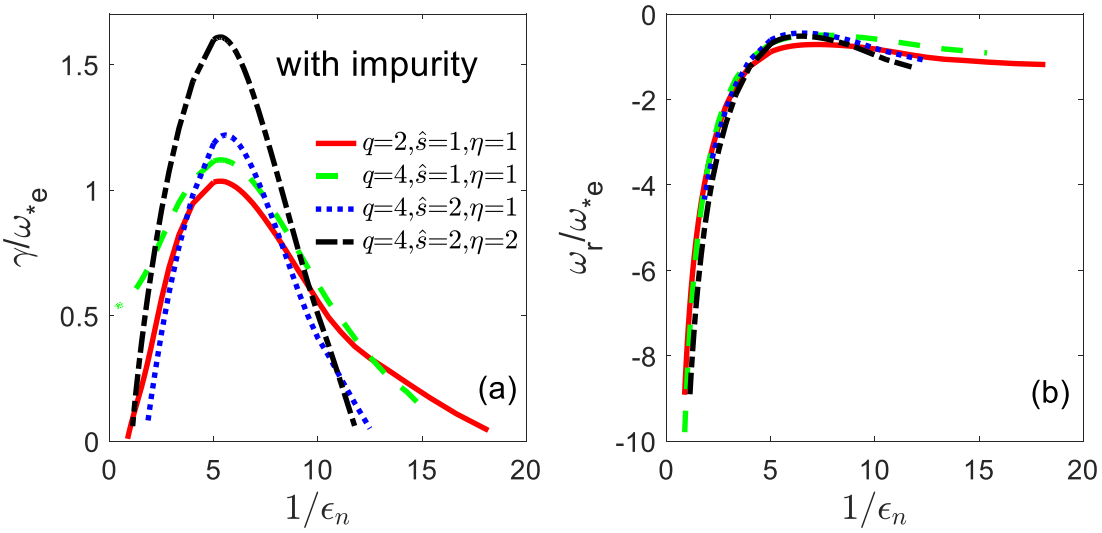

Fig. 5. Dependence of (a) normalized growth rate and (b) real frequency on $1/\varepsilon_n$ for different case of q, $\hat{s}$, and η, the other parameters are $L_{ez} = 1$, $f_z = 0.3$, and C^{6+} impurity ions are considered. For other parameters of each case, please refer to Table I.

$((1/\varepsilon_n) > [1/\varepsilon_n]_{c2})$, it has roughly $\omega_r/\omega_{*e} \sim -2$, as shown in Fig. 4(b).

Comparing Figs. 2 and 4, it can be seen that the electron density gradient $(1/\varepsilon_n)$ is the crucial factor determining the pressure gradient parameters, as is the β (β_e). When $1/\varepsilon_n$ and β (β_e) increase from a value close to 0, respectively, the mode growth rate increases accordingly till reaching the critical value, and the growth rate turns to decrease rapidly with $1/\varepsilon_n$ and β, respectively, until it turns to be 0, where the second KBM stable regime achieves. Corresponding to the critical electron density gradient, the corresponding critical pressure gradient parameter is approximately $\alpha_{c2} \sim 4 - 8$ as shown in Fig. 4(c), which is much lower than what corresponds to the critical β $(\alpha_{c2} \sim 20)$ (see Fig. 2). In Fig. 4, the extended instability can also be seen in the regime of the higher α (generally $\alpha > 3-4$) that causes by the higher electron density gradient, but its instability window is much narrower than that of the extended instability caused by the higher β.

Plotted in Fig. 5 is the dependence of mode eigenvalues on $1/\varepsilon_n$ in the presence of impurities. Comparing Figs. 5 with 4(a) and (b), it can be seen that the presence of impurity reduces the maximum growth rate of each case by nearly one half, and the mode has still a second KBM stable regime of the higher electron density gradient, but its critical value $[1/\varepsilon_n]_{c2}$ is lower than that without impurity [see Fig. 4(a)]. That is to say, the presence of impurities can reduce the threshold for the second stable regime and greatly reduce the instability growth rate of the mode. This implies that it is easier to reach the internal\ external transport barrier threshold by increasing the electron density gradient in the plasma with impurities.

Whether the magnetic shear effect plays a stabilizing or a destabilizing role depends on the shear value $\hat{s}$ related to the safety factor q. Fig. 6(a) and (b) plots the dependences of the mode normalized growth rate and real frequency on $\hat{s}$, respectively. The dependence of the growth rate of each mode on $\hat{s}$ has a turning point, $\hat{s}_c$, where the peak growth rate is located. Only when $\hat{s} > \hat{s}_c$, increasing shear is stabilizing. The maximum growth rate appears at $\hat{s}_c = q/2$, except for the case $q = 4$ and $\eta_i = \eta_e = 1$ (shown with the green dashed line) where $\hat{s}_c \approx q/4$. In addition, the presence of impurities can slightly reduce the critical magnetic shear value, as shown in black dashed-dotted line. In instability studies or actual experiments, when q value is taken large, the corresponding $\hat{s}$ value should also be taken large. The dependence of real frequency on $\hat{s}$ is basically similar for each other. In the range of the mode changing with $\hat{s}$, there is roughly $\omega_r/\omega_{*e} \sim (-6.5, -1)$. When $\hat{s} > \hat{s}_c$, the mode real frequency increases monotonically and rapidly with the increase of $\hat{s}$. The physical basis of the critical magnetic shear for maximum growth rate of KBM is not yet clear. From the present evidence, we know that the critical magnetic shear mainly depends on q value, and $\hat{s}_c \approx q/2$ holds for the normal cases, while this equation can be modified due to other main plasma parameters, such as η_i, β_e and impurity species.

It is interesting that the stabilization (and destabilization) effects of magnetic shear and safety factor on the mode are opposite to each other. Here, it is worth noting that the q effect cannot be inferred by comparing the growth rates between two cases at a fixed $\hat{s}$ in Fig. 6, since in addition to q, there are other key parameters such as β_e that differ between every two cases. In order to accurately study the q effect under the same parameter conditions, we had to insert a subplot in Fig. 6(a) to display the q-dependence of growth rates of two cases at $\hat{s} = 1$. Observing the figure, it is demonstrated evidently when $\hat{s}/q$ is gently less than 1/2 ($\hat{s}/q < 1/4$ is required in some cases), the mode growth rate will increase with $\hat{s}$ while decreases with q, denoting that here the magnetic shear and safety factor play the roles of destabilization and stabilization, respectively. On the contrary, when $\hat{s}/q > 1/2$, the magnetic shear and safety factor play the roles of stabilizing and destabilizing, respectively. However, it is worthy to note that the constraint $q > \hat{s}$ is necessary [see the inserted subplot in Fig. 6(a)] in tokamaks.

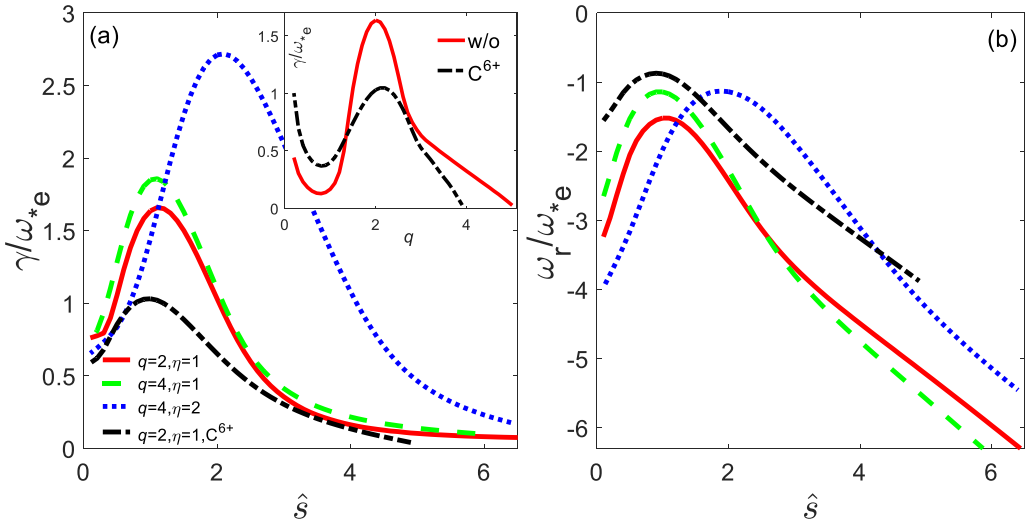

Fig. 6. Dependence of (a) normalized growth rate and (b) real frequency on $\hat{s}$ for different q and η. For comparison, the inserted graph in (a) shows the dependence of the normalized growth rate on q for the cases of $\eta = 1$ and $\hat{s} = 1$, with or without C^{6+} impurity. The other parameters are described in Table I.

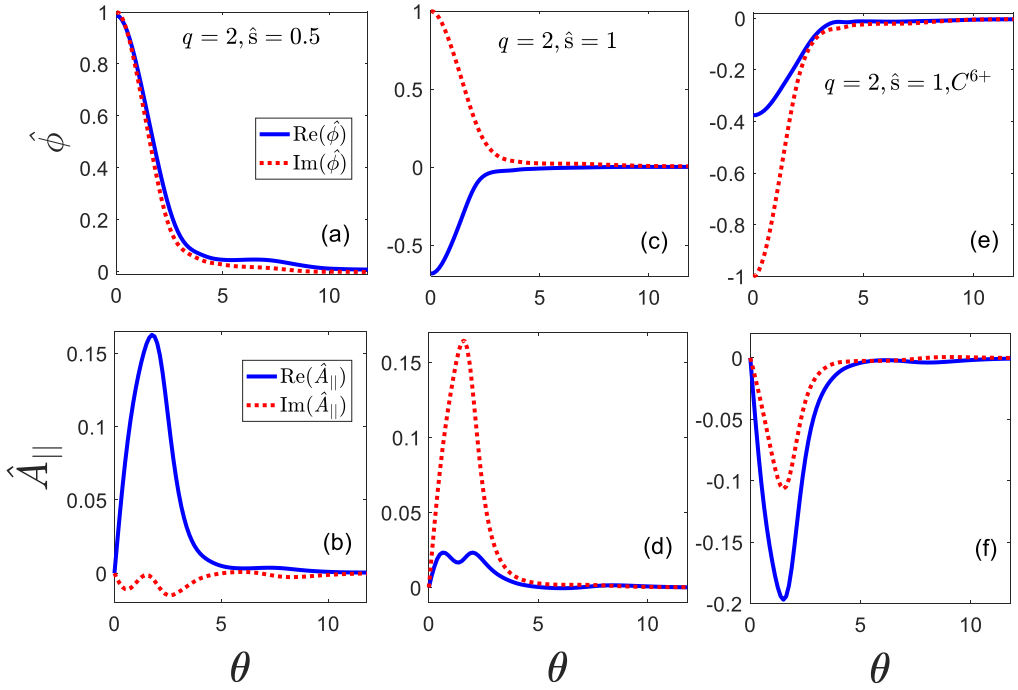

Fig. 7. Mode structures at normalized wavenumber $k_\theta \rho_s = 0.3$: (a) and (b) case $q = 2$ and $\hat{s} = 0.5$ (with $\beta_e = 0.0105$), and $\hat{s} = 1$ (c) and (d) without and (e) and (f) with impurity. Here $\eta_i = \eta_e = 1$. The other parameters of each case are the same as discussed in Table I.

The mode structure reflects one of the fundamental properties of micro-instability. Plotted in Fig. 7 are the mode structures of KBMs at $k_\theta \rho_s = 0.3$ for the cases 2 with $\hat{s} = 0.5$ and $\hat{s} = 1$ with or without impurity. Note that here the mode structure is not plotted in the negative θ region, where the $\hat{\phi}$ and $\hat{A}_{||}$ are even and odd symmetric about the origin point, respectively. It is shown that the principal part of the mode for each case is in the lower θ region, and the potential perturbation is largest at $\theta = 0$. It can be identified that the amplitude of change in mode width is not significant when $\hat{s}$ increases or impurities are present although a small decrease indeed occurs. If carefully observing, we see that as $\hat{s} = 0.5$, the mode width is $\sim 4\pi$ [see Fig. 7(a)]; and for the case $\hat{s} = 1$ without impurity, the mode width is about $\sim 3\pi$ [see Fig. 7(c)]; and as impurities are present [see Fig. 7(e)], the mode width further decreases on a very small scale. On the other hand, the magnetic perturbation remains essentially unchanged for different shear, and the amplitude of the magnetic perturbation increases slightly due to the presence of C^{6+} impurities [see Fig. 7(f)].

IV. Conclusion and Discussion

Many subjects of controlled fusion research cannot be separated from the analysis of the ballooning mode and its stabilization. In this article, the multiple parameter effects

on KBM and its stabilization in tokamaks were qualitatively studied by means of gyrokinetic simulation. The gyrokinetic equations are employed, with FLR, magnetic drift, Landau resonance, and impurity effects being taken into account. The simulation results showed that the ballooning mode has obvious thresholds for the first and second KBM stable region on the electron density gradient, and its thresholds are $[1/\varepsilon_n]_{c1} \sim 1.5-2.5$ for the first KBM stable regime and $[1/\varepsilon_n]_{c2} \sim 12-22$ for the second KBM stable regime for the cases we discussed in the article. Due to the fact that the presence of impurity ions can weaken the compressibility effect, it is observed for the first time that impurity effect is stabilizing on KBMs when the impurity density profile peaks in the same direction as those of the electron and main ion density profiles. The impurity effect will greatly reduce the mode linear growth rate and wavenumber spectrum width [25]. The peak value of KBM growth rate appears at $\hat{s}_c \cong q/4-q/2$, and this formula can be modified due to other main plasma parameters, such as η_i, β_e and impurity species. Besides, the variation of $\hat{s}$ is shown to slightly change the mode structure width and modify the strength of the effects of η_i and impurities on KBMs.

According to the nature of KBM, some favorable factors for stabilizing the mode can be given. First of all, we can consider making the necessary concentration of impurities appear in the plasma, and the higher the q, $\hat{s}$ or η_i (and η_e), the stronger the stabilization effect of the impurities. The second one is to make the pressure gradient reach or close to the second stable regime, one of which is to make the electron density gradient high enough, where the internal or edge transport barrier (ITB/ETB) is anticipated to be formed. Third, one can find the turning point of magnetic shear, $\hat{s}_c$, according to the local parameters, and then try to make $\hat{s}$ decrease or make q increase in the regime of $\hat{s} < \hat{s}_c$, while in the regime $\hat{s} > \hat{s}_c$, increasing the magnetic shear or decreasing the q value is favorable to weaken the mode instability. Here, it is worth noting that the constraint $q > \hat{s}$ is necessary in tokamaks. In our next work, the $\delta B_{||}$ effect will be also included in the integral eigenmode equations and the microscopic instability with complete electromagnetic effects and its influence on transport will be studied.

APPENDIX
DERIVATION OF THE EQUATIONS

The derivation of (13) and (14) is given as follows.

Considering impurity effects, the low-frequency electromagnetic perturbations in inhomogeneous plasmas can be described by quasi-neutral conditions, and the parallel component of Ampere's law

$$\tilde{n}_i + Z\tilde{n}_z = \tilde{n}_e \tag{A1}$$

$$k_\perp^2 \tilde{A}_{||} = \frac{4\pi}{c}\sum_j \tilde{j}_{||}. \tag{A2}$$

Here, $j = e, i, z$. The perturbation density is expressed by $\tilde{n}_j = \int f_j d^3v$, and

$$\tilde{j}_{||} = q_j \int v_{||} f_j d^3v. \tag{A3}$$

Here, $f_j = -(q_j F_{Mj}\tilde{\phi})/T_j + h_j J_0(\delta_j)$, with $F_{Mj} = n_{0j}(\pi v_{tj}^2)^{-(3/2)}\exp(-v^2/v_{tj}^2)$.

By using the gyro-kinetic equation with ballooning mode representation and without considering the plasma shape change, the nonadiabatic response of particles in a circular flux axisymmetric geometric system is satisfied

$$\left(\omega - \omega_{Dj} + i\omega_t \frac{\partial}{\partial\theta}\right)h_j = \left(\omega - \omega_{*Tj}\right)J_0\left(\delta_j\right)F_{Mj}\frac{q_j}{T_j}\left[\tilde{\phi}(\theta) - \frac{v_{||}}{c}\tilde{A}_{||}(\theta)\right]. \tag{A4}$$

Solving (A4), the following results are obtained: if $v_{||} > 0$, then

$$h_j = -iF_{Mj}\frac{n_{oj}q_j}{T_j}\int_{-\infty}^{\theta}\frac{qR}{|v_{||}|}e^{-i\int_\theta^{\theta'}\frac{\omega-\omega_{Dj}(\theta'')}{\omega_t}d\theta''}\left(\omega-\omega_{*Tj}\right) \times J_0\left(\delta\left(\theta'\right)\right)\left[\tilde{\phi}\left(\theta'\right) - \frac{|v_{||}|}{c}\tilde{A}_{||}\left(\theta'\right)\right]d\theta' \tag{A5}$$

else if $v_{||} < 0$, then

$$h_j = -iF_{Mj}\frac{n_{oj}q_j}{T_j}\int_{\theta}^{\infty}\frac{qR}{|v_{||}|}e^{-i\int_\theta^{\theta'}\frac{\omega-\omega_{Dj}(\theta'')}{\omega_t}d\theta''}\left(\omega-\omega_{*Tj}\right) \times J_0\left(\delta\left(\theta'\right)\right)\left[\tilde{\phi}\left(\theta'\right) - \frac{|v_{||}|}{c}\tilde{A}_{||}\left(\theta'\right)\right]d\theta'. \tag{A6}$$

Substitute the nonadiabatic response term h_j into the form $\tilde{n}_j = \int f_j d^3v$, it leads to

$$\tilde{n}_j = -\frac{n_{0j}Z_j e}{T_j}\tilde{\phi} + \int J_0\left(\delta_j\right)h_j d^3v. \tag{A7}$$

And substitute (A7) into the quasi-neutrality condition $\tilde{n}_i + Z\tilde{n}_z = \tilde{n}_e$, we have

$$-\int d^3v J_0(\delta_e)h_e + \int d^3v J_0(\delta_i)h_i + Z\int d^3v J_0(\delta_z)h_z = \frac{n_{0i}e}{T_i}\tilde{\phi} + Z\frac{n_{0z}Ze}{T_z}\tilde{\phi} + \frac{n_{0e}e}{T_e}\tilde{\phi}. \tag{A8}$$

From the quasi-neutrality condition at the equilibrium status

$$n_{0e} = n_{0i} + Zn_{0z}$$

we get

$$\frac{T_e}{n_{0e}e}\times\left[-\int d^3v J_0(\delta_e)h_e + \int d^3v J_0(\delta_i)h_i + Z\int d^3v J_0(\delta_z)h_z\right] = \left[1+\tau_i(1-f_z)+Zf_z\tau_z\right]\tilde{\phi} \tag{A9}$$

thus,

$$\left[1+\tau_i(1-f_z)+Zf_z\tau_z\right]\tilde{\phi} = -\int d^3v J_0(\delta_e)h_e + \int d^3v J_0(\delta_i)h_i + \int d^3v J_0(\delta_z)h_z \tag{A10}$$

that is,

$$\left[1+\tau_i(1-f_z)+Zf_z\tau_z\right]\tilde{\phi} = \int_{-\infty}^{\infty}\left[d\theta' k_{11}^j(\theta,\theta')\tilde{\phi}(\theta') + k_{12}^j(\theta,\theta')\tilde{A}_{||}(\theta')\right] \tag{A11}$$

where

$$k_{ab}^j(\theta,\theta') = -k_{ab}^e(\theta,\theta') + k_{ab}^i(\theta,\theta') + k_{ab}^z(\theta,\theta')$$

with $a, b = 1, 2$. Among them

$$k_{11}^{u}(\theta,\theta') = i\int_0^\infty 2\pi v_\perp dv_\perp \int_0^\infty dv_{||}\frac{qR}{|v_{||}|}\exp\left[i(\beta-\beta')\mathrm{sgn}(\theta-\theta')\right] \times(\omega-\omega_{*Tu})J_0\left(\delta(\theta')\right)J_0(\delta(\theta))F_{Mu} \tag{A12}$$

for $u = i, z$, and

$$\beta-\beta' = \int_{\theta_0}^{\theta} d\theta''\frac{qR}{|v_{||}|}(\omega-\omega_{Du}) - \int_{\theta_0}^{\theta'} d\theta''\frac{qR}{|v_{||}|}(\omega-\omega_{Du}) = (\beta_2-\beta_2')\hat{v}_{||}^{-1} + (\beta_1-\beta_1')\hat{v}_{||} + (\beta_0-\beta_0')\frac{\hat{v}_\perp^2}{\hat{v}_{||}}$$

with

$$\beta_0 = -\int_{\theta'}^{\theta} d\theta''\frac{qR}{2v_{tu}}\hat{\omega}_{Du},\quad \beta_1 = 2\beta_0,\quad \beta_2 = \frac{qR}{v_{tu}}\omega(\theta-\theta').$$

From the above formula, it gives

$$K_{11}^{u}(\theta,\theta') = i\frac{qR}{v_{tu}}\frac{2}{\sqrt{\pi}}\int_0^\infty \hat{v}_\perp d\hat{v}_\perp\int_0^\infty d\hat{v}_{||} \times\exp\left\{\left[i\mathrm{sgn}(\theta-\theta')\right] \times\left[(\beta_2-\beta_2')\hat{v}_{||}^{-1} + (\beta_1-\beta_1')\hat{v}_{||} + (\beta_0-\beta_0')\frac{\hat{v}_\perp^2}{\hat{v}_{||}}\right]\right\} \times(\omega-\omega_{*Tu})J_0(\delta')J_0(\delta)\frac{\exp(-\hat{v}_{||}^2-\hat{v}_\perp^2)}{\hat{v}_{||}} \tag{A13}$$

thus,

$$K_{11}^{u}(\theta,\theta') = \frac{iqR\omega}{2\pi\sqrt{\pi}v_{tu}}\int_{-\infty}^{0} d\theta''\int_{-\infty}^{\infty} d\hat{v}_{||}\int_{-\infty}^{\infty} dt \times\exp\left\{it\left[v_{||}\theta''+(\theta-\theta')\right]\right\} \times\exp\left(-\hat{v}_{||}^2-\frac{iqR\omega}{v_{tu}}\theta''\right)Q'(\hat{v}_{||},\theta,\theta') \tag{A14}$$

where

$$\begin{aligned} Q'(\hat{v}_{||},\theta,\theta') &= \exp\left[i\mathrm{sgn}(\theta-\theta')\right]\left[(\beta_1-\beta_1')\hat{v}_{||}\right] \times\left\{1-\frac{\omega_{*u}}{\omega}\left[1+\eta_u\left(\hat{v}_{||}^2-\frac{3}{2}-\frac{d}{d\lambda}\right)\right]\right\} \times\frac{1}{\lambda}I_0\left(\frac{\sqrt{b_u b_u'}}{\lambda}\right)e^{-\frac{1}{2}\left(\frac{b_u+b_u'}{\lambda}\right)} \\ &= \exp\left[-\frac{i2qR\varepsilon_{nu}\omega_{*u}}{v_{tu}}\mathrm{sgn}(\theta-\theta') \times\left[(1+s)(\sin\theta-\sin\theta') - s(\theta\cos\theta-\theta'\cos\theta')\right] - \frac{\alpha}{2}\left[\theta-\theta'-(\sin\theta\cos\theta-\sin\theta'\cos\theta')\right]\hat{v}_{||}\right] \\ &\quad *\left\{1-\frac{\omega_{*u}}{\omega}\left[\left\{1+\eta_u\left(\hat{v}_{||}^2-\frac{3}{2}+\frac{1}{\lambda}-\frac{b_u+b_u'}{2\lambda^2}\right)\right\}\frac{1}{\lambda}\Gamma_0 + \eta_u\frac{\sqrt{b_u b_u'}}{\lambda^3}\Gamma_1\right]\right\} \end{aligned} \tag{A15}$$

with $\Gamma_0 = I_0(((b_u b_u')^{1/2})/\lambda)e^{-(1/2)((b_u+b_u')/\lambda)}$, $\Gamma_1 = e^{-(1/2)((b_u+b_u')/\lambda)}d/(d\lambda)I_0(((b_u b_u')^{1/2})/\lambda)$.

Perform the integral transformation on (A14) then the following result is obtained:

$$\begin{aligned} K_{11}^{u}(\theta,\theta') &= -i\int_{-\infty}^{0}\frac{\sqrt{2}\ f_u\omega_{*e}}{\sqrt{a_u\lambda_u}(1+a_u)}d\tau\exp(-i\omega\tau) \times\exp\left[-\frac{(k-k')^2}{4\lambda_u}\right] \times\left\{\frac{Z_u\tau_u\omega}{\omega_{*e}} + L_{eu}\left[1-\frac{3}{2}\eta_u+\frac{\eta_u(k-k')^2}{4a_u\lambda_u}\right] + \frac{2\eta_u L_{eu}}{1+a_u} \times\left[1-\frac{\mu_u\left(k_\perp^2+k_\perp'^2\right)}{2(1+a_u)Z_u^2\tau_u} + \frac{\mu_u k_\perp k_\perp'}{(1+a_u)Z_u^2\tau_u}\frac{I_1}{I_0}\right]\right\} \times\Gamma_0(k_\perp,k_\perp'). \end{aligned} \tag{A16}$$

In addition, it gives the second item

$$K_{12}^{u}(\theta,\theta') = i\frac{qR}{v_{tu}}\frac{2}{\sqrt{\pi}}\left(-\frac{|v_{||}|}{c}\right)\int_0^\infty \hat{v}_\perp d\hat{v}_\perp\int_0^\infty d\hat{v}_{||} \times\exp\left\{\left[i\mathrm{sgn}(\theta-\theta')\right]\left[(\beta_2-\beta_2')\hat{v}_{||}^{-1} + (\beta_1-\beta_1')\hat{v}_{||} + (\beta_0-\beta_0')\frac{\hat{v}_\perp^2}{\hat{v}_{||}}\right]\right\} \times(\omega-\omega_{*Tu})J_0(\delta')J_0(\delta)\frac{\exp(-\hat{v}_{||}^2-\hat{v}_\perp^2)}{\hat{v}_{||}}.$$

According to the same treatment method above, finally, we can also get

$$K_{12}^{u}(k,k') = \frac{k-k'}{2\sqrt{a_u\lambda_u}}\cdot\frac{\sqrt{\tau_i}}{\sqrt{\tau_u\mu_u}}K_{11}^{u}(\theta,\theta'). \tag{A17}$$

ACKNOWLEDGMENT

The authors thank G. M. Lv and X.D. Peng for useful discussions.

DATA AVAILABILITY

The data that support the findings of this study are available from the corresponding author upon reasonable request.

REFERENCES

[1] C. Z. Cheng, "High-n collisionless ballooning modes in axisymmetric toroidal plasmas," *Nucl. Fusion*, vol. 22, no. 6, pp. 773–785, Jun. 1982.
[2] B. Coppi, "Thermo-rotational instability in plasma disks around compact objects," *Europhys. Lett.*, vol. 82, no. 1, p. 19001, Apr. 2008.
[3] N. Aiba, "Impact of ion diamagnetic drift on ideal ballooning mode stability in rotating tokamak plasmas," *Plasma Phys. Controlled Fusion*, vol. 58, no. 4, Apr. 2016, Art. no. 045020.
[4] T. C. Hender et al., "MHD stability, operational limits and disruptions," *Nucl. Fusion*, vol. 47, no. 6, p. 128, 1999.
[5] A. Ishizawa, K. Imadera, Y. Nakamura, and Y. Kishimoto, "Global gyrokinetic simulation of turbulence driven by kinetic ballooning mode," *Phys. Plasmas*, vol. 26, no. 8, Aug. 2019, Art. no. 082301.
[6] J. R. Myra, D. A. D'Ippolito, X. Q. Xu, and R. H. Cohen, "Resistive modes in the edge and scrape-off layer of diverted tokamaks," *Phys. Plasmas*, vol. 7, no. 11, pp. 4622–4631, Nov. 2000.
[7] X. Q. Xu, R. H. Cohen, T. D. Rognlien, and J. R. Myra, "Low-to-high confinement transition simulations in divertor geometry," *Phys. Plasmas*, vol. 7, no. 5, pp. 1951–1958, May 2000.

[8] S. Saarelma et al., "Ballooning instability preventing the H-mode access in plasmas with negative triangularity shape on the DIII-D tokamak," *Plasma Phys. Controlled Fusion*, vol. 63, no. 10, Oct. 2021, Art. no. 105006.
[9] T. Eich, R. J. Goldston, A. Kallenbach, B. Sieglin, H. J. Sun, and J. Contributors, "Correlation of the tokamak H-mode density limit with ballooning stability at the separatrix," *Nucl. Fusion*, vol. 58, no. 3, Mar. 2018, Art. no. 034001.
[10] R. J. Hastie and K. W. Hesketh, "Kinetic modifications to the MHD ballooning mode," *Nucl. Fusion*, vol. 21, no. 6, pp. 651–656, Jun. 1981.
[11] A. Hirose, "Skin size ballooning mode in tokamaks," *Plasma Phys. Controlled Fusion*, vol. 49, no. 2, pp. 145–150, Feb. 2007.
[12] K. Itoh, S. Inoue-Itoh, S. Tokuda, and T. Tuda, "Kinetic theory of electromagnetic high-n ballooning instabilities," *Nucl. Fusion*, vol. 22, no. 8, pp. 1031–1047, Aug. 1982.
[13] S. R. Hudson, C. C. Hegna, and N. Nakajima, "Influence of pressure-gradient and shear on ballooning stability in stellarators," *Nucl. Fusion*, vol. 45, no. 4, pp. 271–275, Apr. 2005.
[14] C. H. Ma and X. Q. Xu, "Global kinetic ballooning mode simulations in BOUT++," *Nucl. Fusion*, vol. 57, no. 1, Jan. 2017, Art. no. 016002.
[15] M. Wakatani, "Interchange-ballooning mode in L = 2 helical systems," *IEEE Trans. Plasma Sci.*, vol. PS-9, no. 4, pp. 243–247, Dec. 1981.
[16] A. W. Morris, "MAST: Results and upgrade activities," *IEEE Trans. Plasma Sci.*, vol. 40, no. 3, pp. 682–691, Mar. 2012.
[17] C. Giroud et al., "Progress at JET in integrating ITER-relevant core and edge plasmas within the constraints of an ITER-like wall," *Plasma Phys. Controlled Fusion*, vol. 57, no. 3, Mar. 2015, Art. no. 035004.
[18] M. Willensdorfer et al., "Field-line localized destabilization of ballooning modes in three-dimensional tokamaks," *Phys. Rev. Lett.*, vol. 119, no. 8, Aug. 2017, Art. no. 085002.
[19] J. Q. Xu et al., "Experimental observation of the transition between resistive ballooning modes and ion temperature gradient modes in the edge of the HL-2A tokamak," *Nucl. Fusion*, vol. 58, no. 3, Mar. 2018, Art. no. 036002.
[20] N. Dubuit, O. Agullo, M. Muraglia, J. Frank, X. Garbet, and P. Maget, "Dynamics of magnetic islands driven by ballooning turbulence," *Phys. Plasmas*, vol. 28, no. 2, Feb. 2021, Art. no. 022308.
[21] K. Aleynikova, A. Zocco, P. Xanthopoulos, P. Helander, and C. Nührenberg, "Kinetic ballooning modes in tokamaks and stellarators," *J. Plasma Phys.*, vol. 84, no. 6, Dec. 2018, Art. no. 745840602.
[22] W. M. Tang, G. Rewoldt, C. Z. Cheng, and M. S. Chance, "Kinetic analysis of MHD ballooning modes in tokamaks," *Nucl. Fusion*, vol. 25, no. 2, pp. 151–164, Feb. 1985.
[23] B.-G. Hong, W. Horton, and D.-I. Choi, "Drift-Alfvén kinetic stability theory in the ballooning mode approximation," *Phys. Fluids B: Plasma Phys.*, vol. 1, no. 8, pp. 1589–1599, Aug. 1989.
[24] T. Rhee, G. Y. Park, H. Jhang, S. S. Kim, and R. Singh, "A refined understanding of compressibility effects on the stability of drift ballooning modes," *Phys. Plasmas*, vol. 24, no. 7, Jul. 2017, Art. no. 072504.
[25] Y. Shen, J. Q. Dong, X. D. Peng, M. K. Han, H. D. He, and J. Q. Li, "Extended instability of kinetic ballooning modes induced by ion temperature gradient and impurity in tokamaks," *Nucl. Fusion*, vol. 62, no. 10, Oct. 2022, Art. no. 106004.
[26] J. Y. Kim and H. S. Han, "Kinetic ballooning mode unstable in the 2nd stability regime as a possible source of the low-k broadband fluctuation observed in the wide-pedestal QH-mode," *Nucl. Fusion*, vol. 61, no. 3, Mar. 2021, Art. no. 036048.
[27] A. Bierwage, L. Chen, and F. Zonca, "Pressure-gradient-induced Alfvén eigenmodes: I. Ideal MHD and finite ion Larmor radius effects," *Plasma Phys. Controlled Fusion*, vol. 52, no. 1, Jan. 2010, Art. no. 015004.
[28] I. Condrea, G. Franzoni, and L. Pieroni, "Effect of argon injection on the high Z impurity generation from the poloidal inconel limiter in FTU," *Nucl. Fusion*, vol. 35, no. 7, pp. 787–794, Jul. 1995.
[29] J. Liu et al., "Tungsten impurity effects on the coupling of TEM and ITG mode in reversed magnetic shear tokamak plasmas," *Plasma Phys. Controlled Fusion*, vol. 63, no. 4, Apr. 2021, Art. no. 045004.
[30] C. D. Challis et al., "Effect of q-profile modification by LHCD on internal transport barriers in JET," *Plasma Phys. Control. Fusion*, vol. 43, no. 7, p. 861, 2001.
[31] R. R. Dominguez and G. M. Staebler, "Impurity effects on drift wave stability and impurity transport," *Nucl. Fusion*, vol. 33, no. 1, pp. 51–62, Jan. 1993.
[32] G. M. Staebler et al., "Improved high-confinement mode with neon injection in the DIII-D tokamak," *Phys. Rev. Lett.*, vol. 82, no. 8, pp. 1692–1695, Feb. 1999.
[33] Y. Shen, J. Dong, X. Peng, J. Li, and M. Han, "Numerical study of ubiquitous modes in tokamak plasmas in the presence of impurities," *Plasma Phys. Controlled Fusion*, vol. 62, no. 3, Mar. 2020, Art. no. 035001.
[34] J. W. Connor, R. J. Hastie, and J. B. Taylor, "Shear, periodicity, and plasma ballooning modes," *Phys. Rev. Lett.*, vol. 40, no. 6, pp. 396–399, Feb. 1978.
[35] J. Q. Dong, L. Chen, F. Zonca, and G. D. Jian, "Study of kinetic shear Alfvén instability in tokamak plasmas," *Phys. Plasmas*, vol. 11, no. 3, pp. 997–1005, 2004.
[36] M. Frojdh, M. Liljestrom, and H. Nordman, "Impurity effects on ηi mode stability and transport," *Nucl. Fusion*, vol. 32, no. 3, p. 419, 1992.
[37] J. Q. Dong, W. Horton, and J. Y. Kim, "Toroidal kinetic ηi-mode study in high-temperature plasmas," *Phys. Fluids B: Plasma Phys.*, vol. 4, no. 7, pp. 1867–1876, 1992.

Yong Shen was born in Chongqing, China. He received the bachelor's degree in applied mathematics from Xi'an Jiaotong University, Xi'an, China, in 1992, and the master's and Ph.D. degrees in plasma physics from the Southwestern Institute of Physics, Chengdu, China, in 2005 and 2008, respectively.

He works with the Southwestern Institute of Physics and is honored to be a Professor. Currently, he is engaged in theoretical and simulation research on MHD equilibrium and instability, plasma waves, micro-turbulence, and its transport in tokamak plasmas.

Jia-Qi Dong was born in Yunnan, China. He received the B.Sc. degree from Yunnan University, Kunming, China, in 1966, and the M.Sc. degree from the Southwestern Institute of Physics, Chengdu, China, in 1982.

He cooperated and worked with the University of Maryland at College Park, College Park, MD, USA; the University of Texas at Austin, Austin, TX, USA; the University of California at Irvine, Irvine, CA, USA; the International Center for Theoretical Physics, Trieste, Italy; the National Institute for Fusion Science, Toki, Japan; National Cheng Kung University, Tainan, Taiwan; and the Southwestern Institute of Physics, from 1983 to 1998. Then, he worked with the Southwestern Institute of Physics and was honored to be a Professor and the Head of the Division of Theory and Simulation, in 1998 and 1999, respectively. He was appointed as the Chief Scientist of HL-2A physics experiment in 2010s.

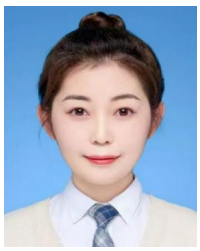

Jia Li was born in Datong, Shanxi, China, in 1993. She received the Ph.D. degree in plasma physics from the School of Physics, Dalian University of Technology, Dalian, China, in 2022.

She currently works as a Lecturer with the School of Mathematics and Science, Chengdu University of Technology, Chengdu, China. She is engaged in theoretical and simulation research on micro-turbulence and its transport in controlled nuclear fusion.